SLEEPJ, 2020, 1–11

doi: 10.1093/sleep/zsaa087
Advance Access Publication Date: 5 May 2020
Original Article

ORIGINAL ARTICLE

Sleep and diurnal rest-activity rhythm disturbances in a mouse model of Alzheimer's disease

Mikolaj J. Filon†, Eli Wallace†, Samantha Wright, Dylan J. Douglas, Lauren I. Steinberg, Carissa L. Verkuilen, Pamela R. Westmark, Rama K. Maganti and Cara J. Westmark*

Department of Neurology, University of Wisconsin–Madison, Madison, WI

*Corresponding author. Cara J. Westmark, Department of Neurology, University of Wisconsin–Madison, Medical Sciences Center, Room 3619, 1300 University Avenue, Madison, WI 53706. Email: westmark@wisc.edu.

†Cofirst authors.

Abstract

Study Objectives: Accumulating evidence suggests a strong association between sleep, amyloid-beta (Aβ) deposition, and Alzheimer's disease (AD). We sought to determine if (1) deficits in rest-activity rhythms and sleep are significant phenotypes in J20 AD mice, (2) metabotropic glutamate receptor 5 inhibitors (mGluR5) could rescue deficits in rest-activity rhythms and sleep, and (3) Aβ levels are responsive to treatment with mGluR5 inhibitors.

Methods: Diurnal rest-activity levels were measured by actigraphy and sleep-wake patterns by electroencephalography, while animals were chronically treated with mGluR5 inhibitors. Behavioral tests were performed, and Aβ levels measured in brain lysates.

Results: J20 mice exhibited a 4.5-h delay in the acrophase of activity levels compared to wild-type littermates and spent less time in rapid eye movement (REM) sleep during the second half of the light period. J20 mice also exhibited decreased non-rapid eye movement (NREM) delta power but increased NREM sigma power. The mGluR5 inhibitor CTEP rescued the REM sleep deficit and improved NREM delta and sigma power but did not correct rest-activity rhythms. No statistically significant differences were observed in Aβ levels, rotarod performance, or the passive avoidance task following chronic mGluR5 inhibitor treatment.

Conclusions: J20 mice have disruptions in rest-activity rhythms and reduced homeostatic sleep pressure (reduced NREM delta power). NREM delta power was increased following treatment with a mGluR5 inhibitor. Drug bioavailability was poor. Further work is necessary to determine if mGluR5 is a viable target for treating sleep phenotypes in AD.

Statement of Significance

Sleep disruption is emerging as an important risk factor as well as the phenotype of neurological diseases including Alzheimer's disease. This study is novel in determining alterations in the rest-activity rhythm and sleep-wake pattern of J20 Alzheimer's disease mice and wild-type littermates. Specifically, there is a delay in acrophase with prolonged hyperactivity during the dark cycle and reduced sleep pressure that was improved by treatment with mGluR5 inhibitor. Critical remaining knowledge gaps and future directions include testing the effects of Alzheimer's disease drugs on the rescue of sleep and rest-activity patterns in other Alzheimer's disease models. These studies are relevant to human Alzheimer's disease as monitoring sleep phenotypes may predict disease risk, and therapies that normalize sleep patterns may slow progression.

Key words: actigraphy; Alzheimer's disease; CTEP; EEG; fenobam; J20 mice; mGluR5; sleep

Submitted: 28 October, 2019; **Revised:** 7 April, 2020

Introduction

Alzheimer's disease (AD) is the sixth most common cause of death in the United States, afflicting approximately 5.4 million Americans, and presents a tremendous emotional and financial hardship on patients and caregivers. AD is a progressive form of dementia characterized histologically by amyloid-beta (Aβ) plaques, neurofibrillary tangles, and neuronal cell death. In a small percentage of cases, AD is directly associated with specific genetic mutations in amyloid-beta protein precursor (AβPP) (chromosome 21), presenilin 1 (chromosome 14), or presenilin 2 (chromosome 1); however, in the vast majority of cases, the cause of the disease is unknown. Patients experience memory loss, impaired judgment, cognitive dysfunction, the inability to perform everyday tasks, and behavioral problems. There are currently no cures for AD, which provides a strong impetus to discover novel therapeutic strategies for treatment and improved outcome measures to bridge preclinical and clinical research.

Deterioration of rest-activity cycles is a progressive phenotype in patients with AD in whom reported sleep disturbances include increased nocturnal awakenings, decreased duration of rapid eye movement (REM) sleep, and diminished slow-wave sleep [1–5]. There is now evidence that rest-activity rhythm fragmentation and sleep disturbances may precede the onset of AD and drive disease pathology [6, 7]. Restlessness, agitation, irritability, and/or confusion worsen in the late afternoon and evening and last into the night with less pronounced symptoms earlier in the day. Thus, we asked if an AD mouse model exhibited altered diurnal rest-activity patterns as determined by actigraphy. We assessed electroencephalogram (EEG)-based sleep-wake patterns to examine correlations between actigraphy and EEG readouts. And, we determined whether any aberration in AD mice could be rescued by modulation of metabotropic glutamate receptor 5 (mGluR5) signaling.

Two classes of drugs, cholinesterase inhibitors (donepezil, rivastigmine, and galantamine) and NMDA receptor antagonists (memantine), are currently approved by the FDA to treat cognitive symptoms of AD. These drugs act on healthy neurons to compensate for lost acetylcholine activity or modulate NMDA receptor activity, respectively. They improve the cognitive ability for a year or less but do not reduce Aβ or neurofibrillary tangle accumulation and subsequent disease progression. Aβ immunotherapy has proven to be very effective in reducing soluble Aβ, amyloid plaque, and soluble tau as well as associated cognitive decline; however, there are questions about safety and it is only experimental at this point [8–11].

An alternative, viable therapeutic target for the treatment of AD may be mGluR5 inhibitors. There is a strong rationale for studying mGluR5 inhibitors in AD models. mGluR5 is a glutamate-activated, G-protein-coupled receptor widely expressed in the central nervous system and clinically investigated as a drug target for a range of indications including depression, Parkinson's disease, and fragile X syndrome (FXS). Amyloid protein precursor (APP) synthesis is regulated through a mGluR5-dependent signaling pathway [12, 13]. The knockout of *mGluR5* in APP_{SWE}/PS1ΔE9 AD mice reduces spatial learning deficits, Aβ oligomer formation, and Aβ plaque number [14]. Treatment with mGluR5 inhibitors reduces APP and Aβ levels and improves memory and cognitive function in mouse models of AD [15–17]. Herein, we test the effects of mGluR5 inhibition on rest-activity rhythms, sleep, locomotor ability, learning and memory, and Aβ levels in J20 mice.

The J20 mouse model is an established rodent model for the study of AD that expresses the human amyloid protein precursor (*hAPP*) gene containing both the Swedish and Indiana familial mutations. J20 mice exhibit greatly exacerbated Aβ production and cognitive deficits [18]. The inclusion of flanking sequences in the transgenic construct is expected to affect posttranscriptional regulation of the *APP* gene and more closely mimic normal temporal and spatial expression of APP and metabolites [19]. Herein, we show that J20 mice exhibited a pronounced 4.5-h shift in acrophase (peak activity levels) during the dark phase of the diurnal cycle and reduced sleep homeostatic pressure as measured by non-rapid eye movement (NREM) delta power. Treatment with mGluR5 inhibitors did not change rest-activity rhythms but CTEP (2-chloro-4-((2,5-dimethyl-1-(4-(trifluoromethoxy)phenyl)-1H-imidazol-4-yl)ethynyl)pyridine) improved NREM delta power with the caveat that therapeutic levels of CTEP were not reached.

Methods

Mouse husbandry

The J20 (B6.Cg-Tg[PDGFB-APPSwInd]20Lms/2Mmjax) mouse model of AD expresses a mutant version of *hAPP* carrying both the Swedish (K670N/M671L) and the Indiana (V717F) mutations directed by the human PDGFB promoter. Hemizygous male J20 mice were purchased from Jackson Laboratories (catalog #006293) and mated with C57BL/6J female mice (Jackson Laboratories, catalog #000664) to generate J20 and wild-type (WT) littermates. Mice were group-housed in microisolator cages on a 06:00 am–06:00 pm light cycle with ad libitum access to food (Teklad 2019) and water. Mouse ages and treatments for specific experiments are defined in the figure legends. The bedding (Shepherd's Cob + Plus, ¼ inch cob) contained nesting material as the only source of environmental enrichment. Drug dosing and testing were conducted in multiple seasons. All animal husbandry and euthanasia procedures were performed in accordance with the National Institutes of Health and an approved University of Wisconsin–Madison IACUC animal care protocol. J20 genotypes were determined by PCR analysis of DNA extracted from tail biopsies with HotStarTaq polymerase (Qiagen, catalog #203205) and Jackson Laboratories' primer sequences oIMR2044 (transgene forward; 5′-GGT GAG TTT GTA AGT GAT GCC-3′) and oIMR2045 (transgene reverse; 5′-TCT TCT TCT TCC ACC TCA GC-3′) targeted at the $APP_{SW/IND}$ transgene (360 base pair [bp] PCR product) and oIMR8744 (internal positive control forward; 5′-CAA ATG TTG CTT GTC TGG TG-3′) and oIMR8745 (internal positive control reverse; 5′-GTC AGT CGA GTG CAC AGT TT-3′), which produce an internal positive control PCR product of 200 bp. J20 mice exhibited a premature mortality phenotype (Supplementary Figure S1), which is consistent with prior studies in Tg2576 [20].

Drug preparation and chronic dosing

Method 1, adult mice. The drugs fenobam (gift from FRAXA Research Foundation), 37.5 mg, and CTEP (2-chloro-4-((2,5-dimethyl-1-(4-(trifluoromethoxy)phenyl)-1H-imidazol-4-yl)ethynyl)pyridine) (MedChem Express, catalog #HY-15445), 5 mg, were transferred into an IKA Ball-Mill Tube BMT-20-S containing 10 stainless steel balls with 7.5 mL 0.9% NaCl, 0.3% Tween-80.

Drug and vehicle were mixed on low velocity for 1 min and high-velocity setting #9 for 5 min. Additional vehicle (7.5 mL) was added and the drug was mixed on high-velocity setting #9 for 5 min. Fenobam stock was 2.5 mg/mL. CTEP was further diluted with 9.75 mL vehicle resulting in final drug concentrations of 0.2 mg/mL CTEP. Vehicle and drugs were frozen in single-use aliquots at –20°C. Mice were dosed once daily with fenobam and once every other day with CTEP at 400 µL per 40 g body weight by oral gavage with 22g 1.4-inch feeding needles with ball ends (Kent Scientific, catalog #FNC-22-1.5). Final drug concentrations were 24 mg/kg fenobam and 2 mg/kg CTEP. Mice were typically dosed midway through the light cycle (11:00 am–01:00 pm).

Method 2, aged mice. CTEP (10 mg) was dissolved in 200 µL DMSO and aliquots at 50 mg/mL were frozen at –20°C. On the day of use, 40 µL of CTEP was mixed with vehicle (1 wt% Hypromellose [HPMC], Sigma catalog #H3785 and 1 wt% Tween-80) in an IKA Ball-Mill Tube BMT-20-S containing 10 stainless steel balls as described above to a final concentration of 0.2 mg/mL CTEP. Mice were dosed at 2 mg/kg by oral gavage.

Neuroassessment

Mice underwent an abbreviated Irwin murine neurobehavioral screen, including weekly weight measurements, at the beginning and end of the drug dosing regimen (Supplementary Tables S1 and S2) [21–23].

Actigraphy

Rest-activity rhythms were assessed under standard lighting conditions in home-made Plexiglas chambers containing passive infrared sensors mounted on the underside of the lids [24, 25]. The dimensions of the transparent cylindrical Plexiglas chambers were 6-inch diameter × 10-inch height. Mice were individually housed during actigraphy with access to food and water. Each gross movement of the animal was recorded as an activity count with VitalView acquisition software (Minimitter Inc., Bend, OR). Activity counts were binned in 60-s epochs and scored on an activity scale (0–50) over a 3- to 9-day period. Data were analyzed with ACTIVIEW Biological Rhythm Analysis software (Mini Mitter Company, Inc.). A chi-square periodogram method was used to determine the diurnal rest-activity period.

EEG sleep analysis

Mice (age 11–12 months old) were recorded in sleep-wake patterns using electroencephalographic monitoring. For EEG electrode implantation surgery (day 1), anesthesia was induced with 5% isoflurane and maintained at 1%–2% in oxygen flowing at 0.5–1 L/min. Three stainless steel epidural screws were placed as electrodes with two screws over the frontal (Bregma +1.5 mm and +1 mm laterally) and parietal cortex (Bregma –3 mm and –1 mm laterally) and one occipital reference (lambda –1 mm at midline). Two stainless steel wire electrodes were placed in the nuchal muscles for electromyography (EMG) recording. The EEG and EMG electrodes were connected to a head cap and secured with dental acrylic. Standard analgesia was administered per local IACUC recommendations. Mice were allowed to recover from the surgery (days 2 and 3, singly housed) prior to transfer to the individual, tethered EEG acquisition chambers and dosing with CTEP (days 4, 6, 8, and 10). EEG recordings and analyses have been previously described [25, 26]. Recordings were acquired days 8–12 on an XLTEK machine (Natus, Madison, WI) with a 512 Hz sampling rate, and the three full days of recordings (days 9–11) were used for the analysis (n = 3–4 mice/treatment cohort). EEG recordings were manually scored in 4-s epochs for REM, NREM, and awake vigilance states with Sirenia Sleep software v.2.0.4 by scorers blinded with respect to treatment group. Waking epochs were identified as those with high EMG amplitude (Supplementary Figure S2A). Epochs with relatively quiescent EMG were scored as sleep. Specific sleep states were differentiated based on predominant EEG power such that NREM was associated with high amplitude delta (1–4 Hz, Supplementary Figure S2B) and REM was associated with low amplitude theta (5–7 Hz, Supplementary Figure S2C) activity.

NREM EEG power among the different treatment groups was analyzed. Power-spectral density was computed for each 4-s segment of 60 Hz notch-filtered EEG using a Fast-Fourier transform, from which power was calculated as integrals of frequencies in delta (0.5–4 Hz), theta (5–9 Hz), sigma (10–14 Hz), and gamma (25–100 Hz) frequency bands. To account for inter-animal variability, EEG power values were normalized to the summed power of delta, theta, sigma, and gamma bands. Records were divided into 2-h bins and the EEG power of NREM epochs within each bin was grouped.

Rotarod

The mice were acclimated to the test room for at least 20 min prior to testing on a Rotarod Treadmill (Med Associates Inc., Vermont). The rotarod was set to a speed setting of 9, which accelerates from 4.0 to 40 rpm over 5 min. Mice were placed on the rotarod and the latency time to when the mouse fell off was recorded. If a mouse made two complete turns hanging onto the grip bar without actively walking/running, the mouse was counted as falling off of the beam. If more than 300 s elapsed, the mouse was removed from the beam. Experiments entailed four trials on day 1 and 2 trials on day 2.

Passive avoidance

Mice were acclimated to the experimental room for at least 20 min prior to testing in a footshock passive avoidance paradigm using an aversive stimulator/scrambler (Med Associates Inc.). A bench-top lamp was turned on behind the center of a light/dark shuttle box and aimed toward the back-left corner away from the dark side of the shuttle box. The power supply on the shock grid was set at 0.6 mA. On the training day, a mouse was placed in the light side of the shuttle box toward the back corner away from the opening to the dark side of the shuttle box. The trap door in the shuttle box was open. After the mouse crossed over to the dark side, the trap door was closed and the latency time for the mouse to move from the light to the dark side was recorded. The mouse was allowed to equilibrate in the dark side for 5 s before receiving a 2-s 0.6 mA footshock. After 15 s, the mouse was removed from the shuttle box and returned to its home cage. The apparatus was cleaned with 70% EtOH between animals. At test times (6, 24, and 48 h after training), the mouse was placed in the light side of the shuttle box facing the left rear corner away from the opening to the dark side with

the trap door open. After the mouse crossed to the dark side, the trap door was closed and the latency time for the mouse to move from the light to the dark side was recorded. If the mouse did not move to the dark side within 300 s, it was gently guided to the dark side and the trap door was closed. The mouse was allowed to equilibrate to the dark side for 5 s before return to the home cage. Mice only received one shock on the training day. Testing at 24 and 48 h measured extinction.

Tissue collection

Mice were treated with isoflurane for 1 min and blood collected from the abdominal artery with a 21G × ¾ inch × 12 inch vacutainer blood collection set (Becton Dickinson, catalog #367296). The blood was immediately mixed with sodium heparin (20 µL of 10 mg/mL; Sigma #H3393). Brain tissues (hippocampus, cerebellum, and right and left cortices) were dissected and quickly frozen on dry ice. Tissue was collected to confirm genotype analyses. The heparinized blood was spun for 10 min at 5,000 rpm at room temperature and the upper plasma layer was transferred to a 1.5 mL Eppendorf tube, frozen on dry ice, and stored at –80°C.

Pharmacokinetics

Plasma and brain left cortices were shipped to Tandem Labs (Durham, NC) for the detection of CTEP levels by mass spectrometry analysis. Study samples were analyzed using standards prepared in sodium heparin mouse plasma. The method calibration range was 0.500–10,000 ng/mL using two different transitions for CTEP. The C13 peak for CTEP was used for the top 5 calibration points and the C12 peak for CTEP was used for the bottom 5 points of the curve. CTEP and fenobam stock solutions for the calibration curve and internal standard, respectively, were prepared at 1 mg/mL in 50:50 water:acetonitrile.

Brain lysates and Aβ ELISA

Diethylamine (DEA) protein extraction buffer (20 µL DEA [0.2% final; Fisher catalog #A11716], 0.5 mL 1M NaCl [50 mM final], 2 mL 10× protease inhibitor cocktail [RPI catalog #P50600] in a 10 mL final volume) was chilled in ice. Tissue to be homogenized (right cortex of the brain) was transferred to a Dounce glass-glass homogenizer with 5 volumes ice-cold DEA protein extraction buffer (1 mL per 200 mg tissue) and homogenized with 35 strokes. Lysates were spun at 20,000*g* for 30 min at 4°C. The cleared supernatant was removed and neutralized with 1/10 volume 0.5M Tris, pH 6.8. Aliquots were quick-frozen at –80°C and protein concentrations quantitated by the BCA Assay (Pierce, catalog #23235) per the manufacturer's instructions. $A\beta_{1-40}$ and $A\beta_{1-42}$ levels were quantitated with Wako Human/Rat Aβ40 (catalog #294–64701) and Wako Human/Rat $A\beta_{1-42}$ high sensitivity (catalog #292–64501) ELISA kits per the manufacturer instructions. Plasma samples were diluted fourfold with standard diluent buffer containing a protease inhibitor cocktail to disrupt interactions between Aβ with masking proteins. Brain samples were diluted 1:50 (WT) and 1:500 (J20) with standard diluent. Antibody-coated plates were incubated with standards and samples overnight at 4°C.

Statistical methods

Statistical significance for peak acrophase comparing two genotypes by three seasons was determined by two-way ANOVA using GraphPad Prism v8.3.0 for Mac OS X (GraphPad Software, San Diego, CA) (Table 1). Statistical significance for peak acrophase and ELISAs comparing two genotypes by two treatments was determined by two-way ANOVA using GraphPad Prism v8.3.0 for Mac OS X (GraphPad Software, San Diego, CA) followed by two-sided *t*-tests using Excel v16.21 software (Supplementary Table S4). Statistical analyses for EEG-based experiments utilized Matlab software (The MathWorks, Inc., Natick, MA) utilizing ANOVAN and multcompare with custom parsing scripts (Supplementary Tables S6–S9). EEG power analysis compared normalized power of delta, theta, sigma, and gamma frequency bands of NREM sleep bouts as determined by manual scoring. As with sleep scoring, all frequency bands were calculated from 4-s epochs of 60 Hz notch-filtered EEG and grouped within 2-h segments across the light cycle. Sleep efficiency was assessed as percent-time in each vigilance state (i.e. wake, NREM, and REM) in four 6-h bins. Both were evaluated using a mixed-model N-way ANOVA using group (i.e. WT-Vehicle, J20-CTEP, etc.) as a fixed-effect variable and time as a random-effect variable. Multiple comparisons were completed with Tukey–Kramer post hoc tests. Each group included in ANOVA analysis was tested for skewness as computed with the skew function in Matlab and satisfied normality with values less than |2|. Statistical analyses were conducted with an α value of 0.05. Cohort sizes varied from n = 6–20 for the actigraphy experiments to n = 3–4 for the EEG and are specified in the figure legends. Means and SEM or 95% confidence intervals are graphed.

Table 1. Mouse Cohorts for Actigraphy Experiments

	WT			J20			
Experiment	N	Age (days)	Peak acrophase (min)	N	Age (days)	Peak acrophase (min)	*t*-test (*p*)
A: fall	15	231 ± 8	836 ± 82	13	232 ± 8	1,081 ± 143	<0.000006
B: winter	20	248 ± 13	941 ± 142	19	244 ± 13	1,041 ± 121	<0.01
C: spring	12	260 ± 5	859 ± 117	8	259 ± 7	1,096 ± 104	<0.0003

Three cohorts of wild-type (WT) and J20 littermate mice were tested by actigraphy during various seasons (set A: fall, set B: winter, set C: spring). A minimum of eight mice were tested per cohort. Average age of the mice was 8 months old (presented in days ± *SD*). Average peak acrophase is the peak activity time in minutes from Zeitgeber time zero ± *SD*. Two-way ANOVA based on season and genotype: interaction $F(2,81) = 3.56$, $p = 0.033$; season $F(2,81) = 0.57$, $p = 0.57$; genotype, $F(1,81) = 49.8$, $p < 0.0001$. One-way ANOVA for WT cohorts as a function of season $F(2,44) = 3.73$, $p = 0.032$. One-way ANOVA for J20 cohorts as a function of season: $F(2,37) = 0.68$, $p = 0.51$. Post hoc *t*-tests for WT: fall versus winter $p = 0.015$, fall versus spring $p = 0.55$, winter versus spring $p = 0.10$.

Results

Rest-activity rhythms are disrupted in J20 mice

Three independent experiments were performed on cohorts of WT and J20 littermate mice at 8 months of age to assess the effect of genotype on rest-activity patterns (Figure 1, Table 1). The experiments were conducted in different seasons (fall, winter, and spring). There was a highly reproducible delay in peak acrophase during the dark cycle in the J20 mice irrespective of the season. Specifically, WT mice exhibited peak activity between 07:00 pm and 08:00 pm, and J20 exhibited peak activity between 11:00 pm and 12:00 am resulting in an approximately 4.5-h delay in acrophase in J20 mice. The findings were consistent in three independent sets of data that compared testing during the fall, winter, and spring, albeit the differences were the most pronounced during the spring followed by the fall and winter. On periodograms, the diurnal period was similar between WT (24.3 ± 0.8; n = 8) and J20 (24.5 ± 0.9; n = 11) mice (p = 0.63). Genotype did not have a significant effect on total daytime activity levels or habituation to the novel actigraphy chambers (Supplementary Figure S3 and Supplementary Table S3).

mGluR5 Inhibitors do not restore rest-activity rhythms in J20 mice

We then tested whether the mGluR5 inhibitors fenobam and CTEP could restore typical rest-activity rhythms. We also performed a behavioral battery along with the actigraphy (Supplementary Figure S4). Mice underwent a pretreatment evaluation of general fitness and grip strength as previously described [21] as well as weekly assessments throughout dosing (Supplementary Table S1 [fenobam] and Supplementary Table S2 [CTEP]). The mGluR5 inhibitors were administered by oral gavage either daily (fenobam) or every other day (CTEP). Neither WT nor J20 mice exhibited alterations in general fitness resulting from treatment. No differences were seen in rest-activity patterns with fenobam (Figure 2). Peak acrophase in the WT and J20 cohorts was similar to the data for the untreated mice (Table 1; Supplementary Table S4). Likewise, CTEP did not alter peak acrophase in WT mice (Figure 3; Supplementary Table S4); however, the stress of chronic injections likely muted the difference between WT and J20 mice (Figure 3, C), which was restored with CTEP (Figure 3, D). We also tested CTEP in aged WT and J20 mice (16- to 19-month-old mice). Neither genotype nor CTEP statistically altered peak acrophase in aged J20 mice (Supplementary Figure S5 and Supplementary Table S4). The average total daily activity counts were not statistically different between WT and J20 mice irrespective of treatment, albeit there were trends for increased activity counts in the J20 mice (Supplementary Table S5). It should be noted that studies in the J20 mice represent the survivors as there was a premature mortality phenotype in the animals (Supplementary Figure S1). Overall, chronic dosing with fenobam and CTEP did not rescue altered rest-activity rhythms in J20 mice.

Analysis of sleep-wake patterns

To quantify the effects of CTEP administration on sleep patterns, EEG was assessed in WT and J20 mice (Figure 4; Supplementary Figure S6). First, 6-h binned mixed-effect ANOVA analyses

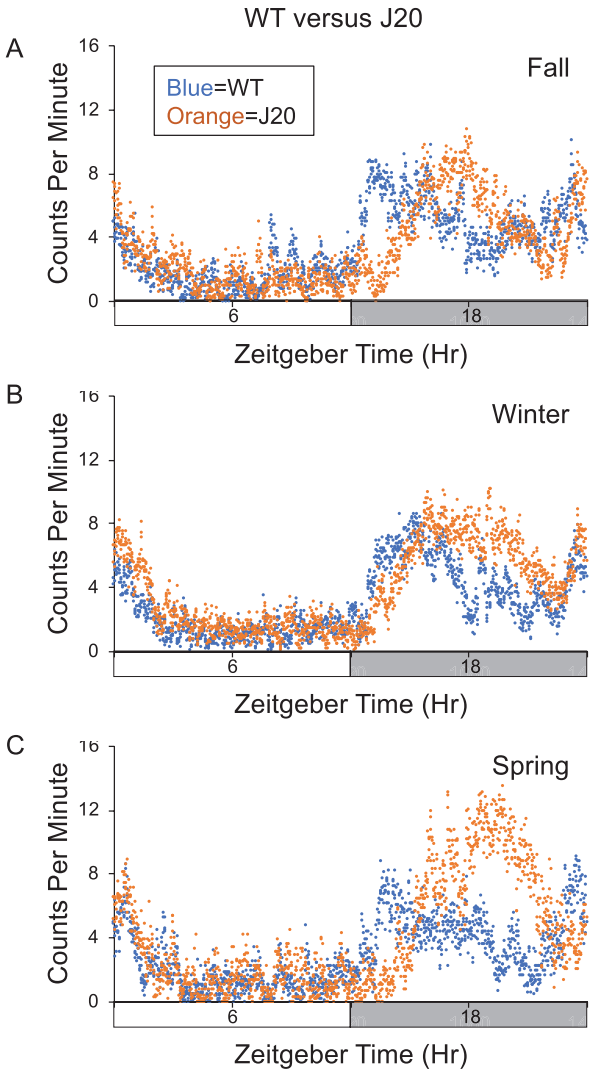

Figure 1. J20 mice exhibit delayed acrophase during the dark cycle. Activity counts on day 1 in the actigraphy chambers were assessed in three separate cohorts of wild-type (WT) (blue) and J20 (orange) 8-month-old mice (A = fall, B = winter, C = spring). Total activity counts (binned in 1 min increments) were averaged for cohorts and plotted on the y-axis versus a 24-h time period (in minutes) on the x-axis. Time zero is "Lights On." (A) Cohort 1 consists of WT (n = 15) and J20 (n = 13). (B) Cohort 2 consists of WT (n = 20) and J20 (n = 19). (C) Cohort 3 consists of WT (n = 12) and J20 (n = 8).

showed a main effect of time in percent time spent for each vigilance state (Supplementary Table S6), suggesting significant oscillation across the light–dark cycle. There was also a main effect of treatment/genotype group in percent awake time (Supplementary Table S6). Multiple comparisons of all interactions (time × group) revealed a significant reduction in an estimated marginal mean of time spent in REM sleep by vehicle-treated J20 (5.3% ± 0.5%) relative to vehicle-treated WT (9.0% ± 0.6%) mice during the second half of the light period, a difference not seen when J20 were treated with mGluR5 inhibitor (Figure 4; Supplementary Table S7).

We then analyzed NREM EEG power among the treatment groups. The oscillation magnitude of EEG delta power in vehicle-treated J20 mice was significantly reduced compared to WT animals treated with vehicle, and there was a delayed dark phase

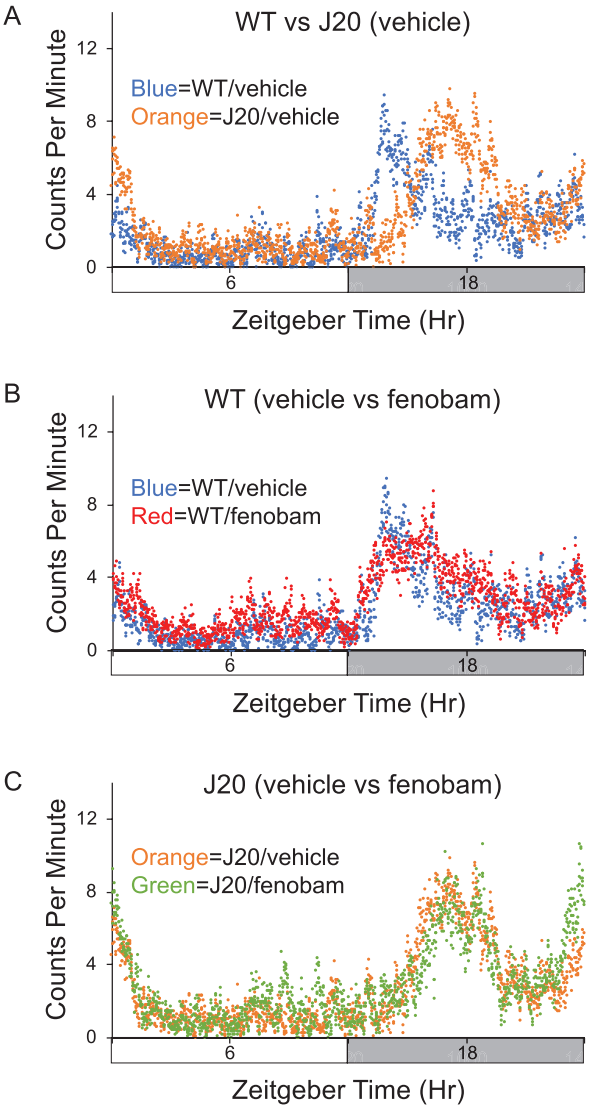

Figure 2. Diurnal activity levels in wild-type (WT) and J20 mice in response to fenobam. Activity counts were assessed in 8-month-old WT and J20 mice after chronic treatment with vehicle or fenobam. Total activity counts (binned in 1 min increments) were averaged over 3–4 days of readings for cohorts and plotted on the *y*-axis versus a 24-h time period (in minutes). Time zero is "Lights On." Cohorts consist of WT mice treated with vehicle (n = 7), J20 treated with vehicle (n = 7), WT treated with fenobam (n = 8), and J20 treated with fenobam (n = 6). (A) vehicle-treated WT (blue) versus J20 (orange). (B) WT mice treated with vehicle (blue) versus fenobam (red). (C) J20 mice treated with vehicle (orange) versus fenobam (green). Mice for these cohorts were tested in fall and winter.

rise, which was similar to the delay in acrophase determined by actigraphy (Figure 5; Supplementary Tables S8 and S9). Of note, treatment with CTEP in J20 mice resulted in a significant increase in delta power, though not to that of WT animals. CTEP appeared to have the opposite effect in WT mice where the overall and oscillation of NREM delta power were reduced compared to vehicle-treated WT animals. Conversely, vehicle-treated J20 mice exhibited consistently increased NREM EEG power in theta and sigma frequency bands (Figure 5, B and C), which was moderately reduced in CTEP-treated J20 animals and increased in CTEP-treated WT animals. Gamma power of NREM sleep showed less consistent differences between vehicle-treated WT and J20 animals (Figure 5, B and C; Supplementary Tables S8 and S9). WT animals showed significantly greater oscillation of NREM gamma power across the day (Figure 5, D; Supplementary Tables S8 and S9). Treatment with CTEP reduced overall NREM gamma power for both genotypes, though the effect was more pronounced in WT animals.

Chronic mGluR5 inhibition does not significantly reduce Aβ levels

There was decreased (32%) plasma $A\beta_{1-40}$ in J20 mice in response to fenobam that was not statistically significant by two-way ANOVA and no other differences in $A\beta_{1-40}$ or $A\beta_{1-42}$ levels observed in plasma or brain for either strain treated with fenobam or CTEP (Supplementary Figure S7). Chronic dosing with fenobam or CTEP did not affect mouse performance in passive avoidance or rotarod testing (Supplementary Figures S8 and S9). Of note, we achieved low bioavailability of CTEP in the mice using established oral gavage dosing protocols. Based on published studies, we expected the dosing regimen to result in a minimal (trough level) drug exposure of 98 ± 14 ng/mL in plasma and 215 ± 28 ng/g in the brain [21–27]; however, we achieved at least a 50-fold lower dose in both blood and brain (Supplementary Figure S10). Poor bioavailability could be due to a variety of factors (Supplementary Text S1).

Discussion

Disruption in rest-activity rhythm and sleep may serve as a disease biomarker in AD [7]. When we examined rest-activity and sleep phenotypes in J20 and WT littermates under diurnal conditions, we found (1) rest-activity rhythms are disrupted in J20 mice as evidenced by altered peak acrophase; and (2) sleep regulation is disrupted in J20 mice as evidenced by reduced NREM EEG delta power, which was partially rescued with CTEP. Our analysis showed that targeting mGluR5 rescued only the sleep phenotype in part but not the rest-activity rhythm or $A\beta_{40}/A\beta_{42}$ levels. Low levels of CTEP bioavailability limit our ability to firmly conclude if CTEP has effects on sleep-activity rhythms or Aβ levels. Since we did not record sleep EEG with fenobam, we cannot comment on its effects on sleep.

J20 mice

There are numerous mouse models available for the study of AD with many exhibiting altered sleep-wake states and diurnal rest-activity rhythms, albeit, there are variations in outcomes among the models [28–33]. Our study is the first, to our knowledge, to directly compare diurnal rest-activity levels to sleep phenotypes in J20 mice. J20 mice are transgenic for the *hAPP* gene with the Swedish 670/671KM-NL and Indiana 717V-F double mutations under regulation by the PDGFβ chain promoter [34]. The transgenic construct contains 70 bases of 5′-UTR, the cDNA, and the 3′-UTR up to the Sph1 site (base 3119 of APP_{695}). The inclusion of flanking sequences in the transgenic construct is expected to affect posttranscriptional regulation of the *APP* gene and temporal and spatial expression of APP and metabolites. J20 mice are devoid of 3D6-immunoreactive Aβ deposits at 2–4 months of age, but amyloid deposition can be observed in 50% of J20 mice by

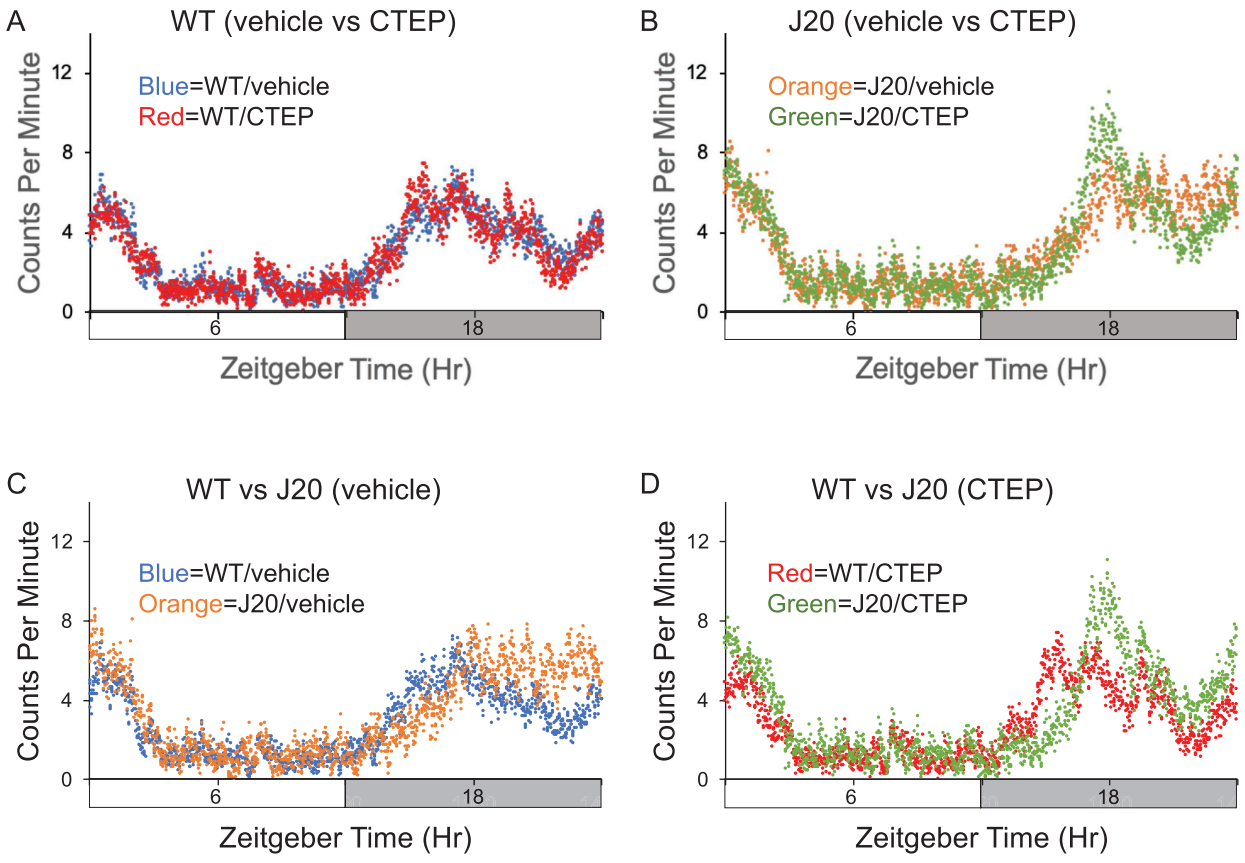

Figure 3. Diurnal activity levels in wild-type (WT) and J20 mice in response to CTEP (2-chloro-4-((2,5-dimethyl-1-(4-(trifluoromethoxy)phenyl)-1H-imidazol-4-yl) ethynyl)pyridine). Activity counts were assessed in 9-month-old WT and J20 mice after chronic treatment with vehicle or CTEP. Total activity counts (binned in 1 min increments) were averaged over 2–4 days of readings for cohorts and plotted on the y-axis versus a 24-h time period (in minutes). Time zero is "Lights On." Cohorts consist of WT mice treated with vehicle ($n = 14$, blue), J20 treated with vehicle ($n = 9$, orange), WT treated with CTEP ($n = 12$, red), and J20 treated with CTEP ($n = 12$, green). (A) WT mice treated with vehicle (blue) versus CTEP (red). (B) J20 mice treated with vehicle (orange) versus CTEP (green). (C) Vehicle-treated WT (blue) versus J20 (orange). (D) CTEP-treated WT (red) versus J20 (green). Mice for these cohorts were tested in winter and spring.

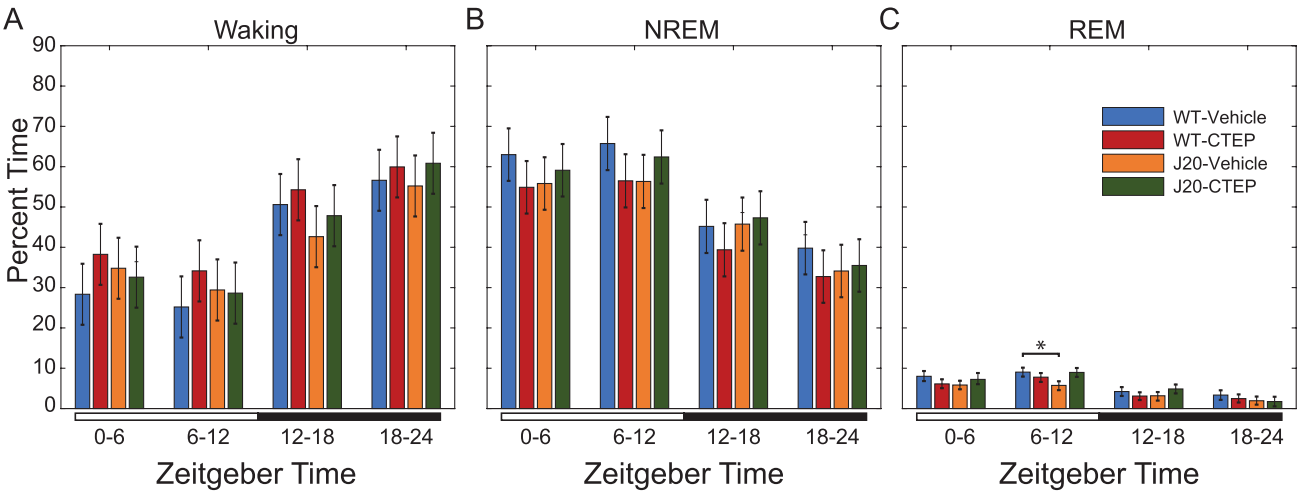

Figure 4. Manually scored sleep based on EEG recordings from wild-type (WT) and J20 mice with and without CTEP. Data were separated into four 6-h bins, starting at Zeitgeber time zero, lights on. The lighting condition is annotated by the bar below the graphs: open: lights on and closed: lights off. Percent time in (A) waking, and (B) NREM and (C) REM sleep are presented as marginal means ± 95% confidence interval (95% CI) for each treatment group: WT treated with vehicle ($n = 3$ mice for 3 days, blue), WT treated with CTEP (2-chloro-4-((2,5-dimethyl-1-(4-(trifluoromethoxy)phenyl)-1H-imidazol-4-yl)ethynyl)pyridine) ($n = 4$ mice for 3 days, red), J20 treated with vehicle ($n = 4$ mice for 3 days, orange), and J20 treated with CTEP ($n = 3$ mice for 3 days, green). Nonoverlapping 95% CI bars indicate a significant difference ($p < 0.05$).

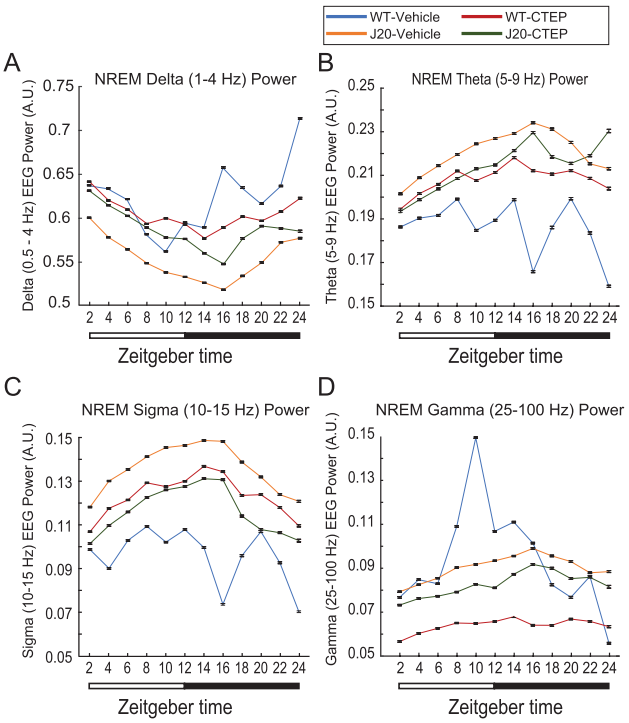

Figure 5. Power spectra of NREM sleep. Electroencephalographic power spectra of 4-s NREM sleep epochs were determined with a fast-Fourier transform. Resulting power of delta (1–4 Hz), theta (5–9 Hz), sigma (10–15 Hz), and gamma (25–100 Hz) frequencies was isolated and normalized to the summed power of all frequency bands. Each 24-h recording was divided into 2-h segments, and manually scored NREM epochs within each bin were grouped. Here, normalized (A) delta, (B) theta, (C) sigma, and (D) gamma powers are presented as mean ± 95% confidence interval (CI) for each treatment group: wild type (WT) treated with vehicle (n = 3 mice for 3 days, blue); J20 treated with vehicle (n = 4 mice for 3 days, orange); WT treated with CTEP (2-chloro-4-((2,5-dimethyl-1-(4-(trifluoromethoxy) phenyl)-1H-imidazol-4-yl)ethynyl)pyridine) (n = 4 mice for 3 days, red); and J20 treated with CTEP (n = 3 mice for 3 days, green). Nonoverlapping CI bars indicate a significant difference ($p < 0.05$). Lighting conditions are shown below the graph. Mixed-model ANOVA statistics are provided in Supplementary Table S7.

5–7 months of age and in 100% of mice by 8–10 months (human equivalent, 42–50 years old) [34, 35].

J20 mice exhibit an altered rest-activity rhythm characterized by a 4-h shift in the acrophase of peak activity, delays in activity onset and activity offset, and increased total activity during the dark cycle. Activity onset is a measure of the time of day in which the animals begin their most active period, and activity offset is a measure of when this active period ends. Since rodents are nocturnal, activity onset should begin at or around the start of the dark phase [36]. Our findings are consistent with clinical studies showing later acrophase in patients with AD [37–39]. J20 mice are hyperactive in the open field and exhibit reduced anxiety [40, 41]. However, we did not find a significant increase in total activity or decreased habituation to the novel actigraphy environment.

The EEG-based analysis showed minimal differences in time spent in NREM and REM sleep, but a profound decrease in NREM EEG-delta power in J20 mice. Specifically, with regard to REM, vehicle-treated J20 mice have a lower marginal mean (a weighted estimate of population means) of percent time spent in REM sleep from Zeitgeber time (ZT) 6–12 h compared to vehicle-treated WT animals, which is rescued by CTEP in J20 mice. According to the two-process model of sleep introduced by Borbély, sleep is regulated by both circadian and homeostatic mechanisms [42]. The latter has been described as the pressure for sleep that grows during periods of wakefulness and is expunged by NREM sleep. Delta power is a commonly employed correlate of homeostatic sleep pressure, normally decreasing across the light period when mice are mainly resting and increasing with activity across the active dark period [43, 44]. This relationship between activity and EEG delta power of NREM sleep is evidenced by substantial increases in delta (1–4 Hz) EEG power following brief (4 h) total sleep deprivation in mice [43]. Our findings agree with previous murine AD studies demonstrating a decrease in delta band EEG power, while the activity of higher frequencies is increased [45]. This apparent shift may be due to the large decreases in J20 NREM delta power, which has the largest influence on the power normalization, but it may also be indicative of hyperexcitability of neurons contributing to activity outside the typical on-off periods underlying high-amplitude, slow activity recorded at cortical surfaces during NREM sleep [46]. Importantly, the increase in delta power occurs later in the subjective day, and it can be assumed that it increases in proportion to the delayed waking duration and associated intensity of activity in J20 mice. It appears that CTEP treatment improves NREM delta power (sleep pressure), although it reduces oscillatory amplitude in both WT and J20. Overall, the cyclic decay and accrual of delta power across the 24-h period fit reasonably well with actigraphy, suggesting its viability as a substitute diagnostic tool for AD in place of invasive EEG-based methods. Taken together with delayed acrophase in locomotor activity observed by actigraphy during the dark phase, the phase-shifted NREM delta power may indicate a perturbed function of the central pacemaker, affecting typical consolidation of sleep to subjectively appropriate times of the day.

mGluR5 inhibition

All of the currently approved drugs for the treatment of AD act on healthy neurons to compensate for lost acetylcholine activity in the case of cholinesterase inhibitors or to modulate NMDA receptor activity in the case of memantine. They improve the cognitive ability for a year or less but do not reduce Aβ accumulation or subsequent disease progression. The therapeutic potential of targeting mGluR5 in AD has been reviewed [47]. *App* mRNA is a synaptic target for regulation by FMRP and mGluR5. Activation of mGluR5 signaling induces the release of the translational repressor FMRP from *App* mRNA and the subsequent synthesis of AβPP [12]. Excessive AβPP production favors amyloidogenic processing and the production of Aβ. Aβ disrupts human NREM slow waves and related hippocampus-dependent memory consolidation [48]. We have observed that treatment with the mGluR5 inhibitor CTEP partly rescued the sleep phenotype, which has not been previously reported to our knowledge. There is evidence that $mGluR_5$ may have a modulatory role in the molecular machinery of sleep homeostasis [49]. Thus, $mGluR_5$ inhibitors may affect sleep-wake patterns but further study into the mechanism is required. Whether this translates to improved cognition remains to be determined.

Fenobam and CTEP are potent and highly selective noncompetitive inhibitors of mGluR5 [27, 50, 51]. CTEP has a 30- to 100-fold higher in vivo potency compared to MPEP and fenobam and is 1,000-fold more selective for mGluR5 when

compared to 103 molecular targets including all known mGluRs [27]. Thus, if fenobam and/or CTEP are proven effective in reducing Aβ accumulation and the cognitive decline associated with AD, mGluR5 inhibitors could provide an alternative, orally administered treatment for AD, which lack the problems associated with antibody-based therapies. The dose of fenobam used herein (24 mg/kg/day) was calculated based on published rodent and human pharmacokinetic data. Phase I dose-escalation trials showed safety and a lack of cognitive dysfunction in humans receiving up to 8–9 mg/kg/day fenobam for 3 weeks [52]. Thus, the dose is threefold higher than that safely tested in humans, but far less than that safely tested in rats [53]. Chronic dosing for 10 weeks at this dose resulted in no adverse side effects on weight gain or home cage behavior [15]. As there are no reports of toxicity with the drug, we proposed to err on the side of overdosing to ascertain fenobam effects on learning and memory and biomarker expression. CTEP is the first reported mGluR5 inhibitor with both a long half-life of approximately 18 h and high oral bioavailability, allowing chronic treatment with continuous receptor blockade with one dose every 48 h in adult animals [27]. Chronic treatment (2 mg/kg every 48 h) inhibits mGluR5 with a receptor occupancy of 81% and rescues cognitive deficits in *Fmr1*^{KO} mice [21]. For this study, we dosed by oral gavage as published pharmacokinetic data by this method are available in other rodent models [21, 27].

Treatment with mGluR5 inhibitors, fenobam or CTEP, did not rescue altered rest-activity profiles, affect mouse performance in rotarod or passive avoidance testing, or decrease Aβ levels, although there were modest improvements in NREM delta power in CTEP-treated J20 mice. Oddly, oral gavage with vehicle shifts peak acrophase in WT mice. Specifically, in Figure 3, B with oral gavage every 48 h, average peak acrophase occurs at least 1 h later in the WT mice, thus attenuating differences observed between WT and J20 in the absence of restraint/oral gavage (Figure 1). Increased activity in J20 is observed at the end of the dark phase. This is a finding that we could not explain. The actigraphy and behavioral analyses involved chronic dosing with CTEP over 30 days whereas the EEG involved treatment for 1 week. Drug tolerance with mGluR5 inhibitors has been raised as an issue in failed FXS clinical trials [54]. Consistent with chronic dosing studies of fenobam as a feed supplement in AD mice (Tg2576 and R1.40^{HET}), and with chronic dosing of CTEP by oral gavage in FXS mice (*Fmr1*^{KO}) [15, 21], we observed normal weight gain, motor activity, grooming, and home-cage behavior with no adverse side effects. In contrast, genetic reduction of mGluR5 or chronic oral administration of CTEP rescues spatial learning deficits in APP_{SWE}/PS1dE9 mice [14, 17], and BMS-984923 mGluR5 inhibitor treatment rescues memory deficits and synaptic depletion in APP_{SWE}/PS1dE9 mice [55]. We did not find genotype or drug-dependent effects on learning and memory by passive avoidance in J20 mice. Prior chronic dosing studies with fenobam in AD model mice reduced Aβ levels [15]; however, those mice were dosed with a feed supplement and here we had poor bioavailability by oral gavage.

Study limitations

Limitations of the study include poor bioavailability and possibly drug tolerance of the mGluR5 inhibitors, the use of one AD mouse model, mice are nocturnal, and the oral gavage procedure shifts peak acrophase in WT mice. To begin to address these issues, future studies can include the administration of drugs as feed supplements, testing the effects of drugs that modulate Aβ production such as β-secretase inhibitors, and determination of diurnal activity and sleep patterns in additional AD mouse models.

Conclusions

Sleep disturbances and behavioral symptoms are the main reasons to institutionalize patients with AD [56, 57]. We observed disruptions in rest-activity rhythms and sleep in J20 mice, and sleep was partially rescued with one mGluR5 inhibitor. Chronic treatment with mGluR5 inhibitors did not rescue rest-activity rhythms or Aβ levels in J20 mice, but altered dosing administration methods or alternative drugs may be effective and deserve further investigation. Actigraphy was a reasonable surrogate for EEG with the noted limitations. Overall, targeting sleep may be an avenue to delay the development and/or progression of AD.

Supplementary Material

Supplementary material is available at *SLEEP* online.

Acknowledgments

We thank Dr Andrzej Dekundy (Merz Pharmaceuticals GmbH) and Dr Lothar Lindemann (F. Hoffmann-La Roche) for advice on CTEP inhibitor solubility.

Funding

This research was supported by National Institute on Aging grant AG044714, the University of Wisconsin–Madison Alzheimer's Disease Research Center (ADRC) grant P50-AG033514, the Clinical and Translational Science Award (CTSA) program through the National Center for Advancing Translational Sciences (NCATS) grant UL1TR002373, the Department of Defense (DOD) grant W81XWH-16-1-0082, and FRAXA Research Foundation.

Disclosure Statement

Financial Disclosure: None.

Nonfinancial Disclosure: None.

Prior deposit of manuscript in a Preprint database: BioRxiv.

Ethical Statement

All mouse procedures were performed in accordance with the NIH guidelines and an approved University of Wisconsin–Madison animal care protocol administered through their Institutional Animal Care and Use Committee.

Conflict of interest statement. None declared.

References

1. Hatfield CF, *et al*. Disrupted daily activity/rest cycles in relation to daily cortisol rhythms of home-dwelling patients with early Alzheimer's dementia. *Brain*. 2004;**127**:1061–1074.

2. Prinz PN, *et al*. Changes in the sleep and waking EEGs of nondemented and demented elderly subjects. *J Am Geriatr Soc*. 1982;**30**:86–93.
3. Petit D, *et al*. Sleep and quantitative EEG in neurodegenerative disorders. *J Psychosom Res*. 2004;**56**:487–496.
4. Martin PR, *et al*. Sleep EEG in Korsakoff's psychosis and Alzheimer's disease. *Neurology*. 1986;**36**:411–414.
5. Loewenstein RJ, *et al*. Disturbances of sleep and cognitive functioning in patients with dementia. *Neurobiol Aging*. 1982;**3**:371–377.
6. Musiek ES, *et al*. Sleep, circadian rhythms, and the pathogenesis of Alzheimer disease. *Exp Mol Med*. 2015;**47**:e148.
7. Musiek ES, *et al*. Circadian rest-activity pattern changes in aging and preclinical Alzheimer disease. *JAMA Neurol*. 2018;**75**:582–590.
8. Morgan D. Mechanisms of A beta plaque clearance following passive A beta immunization. *Neurodegener Dis*. 2005;**2**:261–266.
9. Check E. Nerve inflammation halts trial for Alzheimer's drug. *Nature*. 2002;**415**:462.
10. Pfeifer M, *et al*. Cerebral hemorrhage after passive anti-Abeta immunotherapy. *Science*. 2002;**298**:1379.
11. Racke MM, *et al*. Exacerbation of cerebral amyloid angiopathy-associated microhemorrhage in amyloid precursor protein transgenic mice by immunotherapy is dependent on antibody recognition of deposited forms of amyloid beta. *J Neurosci*. 2005;**25**:629–636.
12. Westmark CJ, *et al*. FMRP mediates mGluR5-dependent translation of amyloid precursor protein. *PLoS Biol*. 2007;**5**:e52.
13. Westmark CJ. Fragile X and APP: a decade in review, a vision for the future. *Mol Neurobiol*. 2019;**56**:3904–3921.
14. Hamilton A, *et al*. Metabotropic glutamate receptor 5 knockout reduces cognitive impairment and pathogenesis in a mouse model of Alzheimer's disease. *Mol Brain*. 2014;**7**:40.
15. Malter JS, *et al*. Fragile X Syndrome and Alzheimer's disease: another story about APP and beta-amyloid. *Curr Alzheimer Res*. 2010;**7**:200–206.
16. Westmark PR, *et al*. Rescue of Fmr1KO phenotypes with mGluR5 inhibitors: MRZ-8456 versus AFQ-056. *Neurobiol Dis*. 2018;**119**:190–198.
17. Hamilton A, *et al*. Chronic pharmacological mglur5 inhibition prevents cognitive impairment and reduces pathogenesis in an Alzheimer disease mouse model. *Cell Rep*. 2016;**15**:1859–1865.
18. Palop JJ, *et al*. Aberrant excitatory neuronal activity and compensatory remodeling of inhibitory hippocampal circuits in mouse models of Alzheimer's disease. *Neuron*. 2007;**55**:697–711.
19. Westmark CJ, *et al*. APP causes hyperexcitability in fragile X mice. *Front Mol Neurosci*. 2016;**9**:147.
20. Westmark CJ, *et al*. Seizure susceptibility and mortality in mice that over-express amyloid precursor protein. *Int J Clin Exp Pathol*. 2008;**1**:157–168.
21. Michalon A, *et al*. Chronic pharmacological mGlu5 inhibition corrects fragile X in adult mice. *Neuron*. 2012;**74**:49–56.
22. Higgins GA, *et al*. Influence of the selective ORL1 receptor agonist, Ro64-6198, on rodent neurological function. *Neuropharmacology*. 2001;**41**:97–107.
23. Irwin S. Comprehensive observational assessment: Ia. A systematic, quantitative procedure for assessing the behavioral and physiologic state of the mouse. *Psychopharmacologia*. 1968;**13**:222–257.
24. Fenoglio-Simeone KA, *et al*. Ketogenic diet treatment abolishes seizure periodicity and improves diurnal rhythmicity in epileptic Kcna1-null mice. *Epilepsia*. 2009;**50**:2027–2034.
25. Wallace E, *et al*. Differential effects of duration of sleep fragmentation on spatial learning and synaptic plasticity in pubertal mice. *Brain Res*. 2015;**1615**:116–128.
26. Wallace E, *et al*. Altered circadian rhythms and oscillation of clock genes and sirtuin 1 in a model of sudden unexpected death in epilepsy. *Epilepsia*. 2018;**59**:1527–1539.
27. Lindemann L, *et al*. CTEP: a novel, potent, long-acting, and orally bioavailable metabotropic glutamate receptor 5 inhibitor. *J Pharmacol Exp Ther*. 2011;**339**:474–486.
28. Huitrón-Reséndiz S, *et al*. Sleep-wake states in transgenic mouse models overexpressing the human beta-amyloid precursor protein. *Am J Alzheimers Dis Other Demen*. 2005;**20**:87–90.
29. Wisor JP, *et al*. Sleep and circadian abnormalities in a transgenic mouse model of Alzheimer's disease: a role for cholinergic transmission. *Neuroscience*. 2005;**131**:375–385.
30. Huitrón-Reséndiz S, *et al*. Age-independent and age-related deficits in visuospatial learning, sleep-wake states, thermoregulation and motor activity in PDAPP mice. *Brain Res*. 2002;**928**:126–137.
31. Colby-Milley J, *et al*. Sleep-wake cycle dysfunction in the TgCRND8 mouse model of Alzheimer's disease: from early to advanced pathological stages. *PLoS One*. 2015;**10**(6):e0130177.
32. Kent BA, *et al*. Delayed daily activity and reduced NREM slow-wave power in the APPswe/PS1dE9 mouse model of Alzheimer's disease. *Neurobiol Aging*. 2019;**78**:74–86.
33. Van Erum J, *et al*. Sleep architecture changes in the APP23 mouse model manifest at onset of cognitive deficits. *Behav Brain Res*. 2019;**373**:112089.
34. Mucke L, *et al*. High-level neuronal expression of abeta 1-42 in wild-type human amyloid protein precursor transgenic mice: synaptotoxicity without plaque formation. *J Neurosci*. 2000;**20**:4050–4058.
35. Beauquis J, *et al*. Neuronal and glial alterations, increased anxiety, and cognitive impairment before hippocampal amyloid deposition in PDAPP mice, model of Alzheimer's disease. *Hippocampus*. 2014;**24**:257–269.
36. Boggs KN, *et al*. Circadian wheel running behavior is altered in an APP/E4 mouse model of late onset Alzheimer's disease. *Physiol Behav*. 2017;**182**:137–142.
37. Little JT, *et al*. Sundown syndrome in severely demented patients with probable Alzheimer's disease. *J Geriatr Psychiatry Neurol*. 1995;**8**:103–106.
38. Satlin A, *et al*. Circadian locomotor activity and core-body temperature rhythms in Alzheimer's disease. *Neurobiol Aging*. 1995;**16**:765–771.
39. Volicer L, *et al*. Sundowning and circadian rhythms in Alzheimer's disease. *Am J Psychiatry*. 2001;**158**:704–711.
40. Flores J, *et al*. Caspase-1 inhibition alleviates cognitive impairment and neuropathology in an Alzheimer's disease mouse model. *Nat Commun*. 2018;**9**:3916.
41. Fujikawa R, *et al*. Deficiency in EP4 receptor-associated protein ameliorates abnormal anxiety-like behavior and brain inflammation in a mouse model of Alzheimer disease. *Am J Pathol*. 2017;**187**:1848–1854.
42. Borbély AA, *et al*. The two-process model of sleep regulation: a reappraisal. *J Sleep Res*. 2016;**25**:131–143.
43. Nelson AB, *et al*. Sleep patterns and homeostatic mechanisms in adolescent mice. *Brain Sci*. 2013;**3**:318–343.
44. Easton A, *et al*. The suprachiasmatic nucleus regulates sleep timing and amount in mice. *Sleep*. 2004;**27**:1307–1318.

45. Kent BA, *et al*. Sleep and EEG power spectral analysis in three transgenic mouse models of Alzheimer's disease: APP/PS1, 3xTgAD, and Tg2576. *J Alzheimers Dis*. 2018;**64**:1325–1336.
46. Nir Y, *et al*. Regional slow waves and spindles in human sleep. *Neuron*. 2011;**70**:153–169.
47. Kumar A, *et al*. Therapeutic potential of mGluR5 targeting in Alzheimer's disease. *Front Neurosci*. 2015;**9**:215.
48. Mander BA, *et al*. β-amyloid disrupts human NREM slow waves and related hippocampus-dependent memory consolidation. *Nat Neurosci*. 2015;**18**:1051–1057.
49. Holst SC, *et al*. Cerebral mGluR5 availability contributes to elevated sleep need and behavioral adjustment after sleep deprivation. *ELife*. 2017;**6**:e28751.
50. Wållberg A, *et al*. Phenyl ureas of creatinine as mGluR5 antagonists. A structure-activity relationship study of fenobam analogues. *Bioorg Med Chem Lett*. 2006;**16**:1142–1145.
51. Porter RH, *et al*. Fenobam: a clinically validated nonbenzodiazepine anxiolytic is a potent, selective, and noncompetitive mGlu5 receptor antagonist with inverse agonist activity. *J Pharmacol Exp Ther*. 2005;**315**:711–721.
52. Lapierre Y, *et al*. Fenobam: another anxiolytic? *Curr Ther Res*. 1982;**31**:95–101.
53. Wu WN, *et al*. In vitro and in vivo metabolism of the antianxiolytic agent fenobam in the rat. *J Pharm Sci*. 1995;**84**(2):185–189.
54. McCamphill PK, *et al*. Understanding and overcoming pharmacological tolerance in the treatment of fragile X syndrome. *Soc Neurosci*. 2019; Abstract #366.18.
55. Haas LT, *et al*. Silent allosteric modulation of mGluR5 maintains glutamate signaling while rescuing Alzheimer's mouse phenotypes. *Cell Rep*. 2017;**20**:76–88.
56. Pollak CP, *et al*. Sleep problems and institutionalization of the elderly. *J Geriatr Psychiatry Neurol*. 1991;**4**:204–210.
57. Vecchierini MF. Sleep disturbances in Alzheimer's disease and other dementias. *Psychol Neuropsychiatr Vieil*. 2010;**8**:15–23.